JOURNAL OF CATALYSIS **158,** 311–326 (1996)
ARTICLE NO. 0030

Studies on the Catalytic Activity of Zirconia Promoted with Sulfate, Iron, and Manganese

Kam T. Wan, Charles B. Khouw, and Mark E. Davis[1]

Division of Chemistry and Chemical Engineering, California Institute of Technology, Pasadena, California 91125

Received June 6, 1995; revised September 12, 1995

The catalytic properties of iron- and manganese-promoted sulfated zirconia (SFMZ) for the isomerization of *n*-butane to isobutane are investigated using various catalyst pretreatments and reaction conditions. The *n*-butane isomerization reactivity at 30°C is effected by calcination of the catalyst at 650°C in helium and vacuum treatment at room temperature indicating that superacidity is not likely to be responsible for activity. In addition, SFMZ samples exposed to dry air at over 450°C are more active than those calcined in helium at a reaction temperature of 30°C (*n*-butane conversions of 18.7% vs 0.4%) suggesting the presence of an active site involving a metal "oxy" species. The oxy species is capable of reacting CO to CO_2 at room temperature and is present at a number density of 10–15 μmol/g. At a reaction temperature of 100°C, SFMZ catalysts calcined in air then activated in helium show similar reactivities to those activated in air up to a preheating temperature of 450°C; above 450°C the metal oxy species is formed and provides additional activity (*n*-butane conversions of 37.1% in air vs 15.4% in He for calcinations at 650°C). The nature of the active sites on SFMZ are investigated using temperature-programmed desorption of substituted benzenes. The liberation of CO_2 and SO_2 in the benzene TPD profile of SFMZ is attributed to the oxidation of benzene at the redox-active metal sites, resulting in the subsequent decomposition of the reduced iron (II) sulfate. Data from the TPD studies do not suggest the presence of superacidity on SFMZ that could contribute to the low-temperature *n*-butane isomerization activity. Instead, a bifunctional mechanism that involves a combination of a redox-active metal site and an acid site in close proximity is proposed.

INTRODUCTION

Large-scale isomerization of *n*-butane is currently accomplished with a Pt on chlorinated alumina catalyst, while HF or H_2SO_4 is used as catalyst for aliphatic alkylation (1–3). Although these catalysts accomplish these reactions with great efficacy, they pose hazardous environmental problems for disposal. Therefore, there is a great incentive for developing new solid noncontaminant catalysts (4–6). Since the isomerization of *n*-butane and the alkylation of isobutane with light alkenes are catalyzed by strong acids, nonhalide solid acid catalysts could be possible solutions to the environmental problems provided they are able to promote the hydrocarbon conversions with high activity/selectivity and lifetime. As the transformation of *n*-butane to isobutane is thermodynamically favored at low reaction temperatures, very strong acid catalysts that can carry out this reaction at low temperatures could be particularly effective. Among the various well-known inorganic acids, e.g., zeolites (7–9), silica–aluminas (10), and heteropoly-acids (11, 12), sulfated oxides, particularly zirconia, have received attention (13–24). Initially sulfated zirconia was considered to be a superacid, i.e., having an acid strength stronger than that of 100% sulfuric acid (5). However, this point of view has recently been questioned (25–28). Sulfated zirconia has been shown to be very active for *n*-butane isomerization at high temperature. Unfortunately, relatively rapid deactivation accompanies the isomerization (29, 30) and a lack of regenerability is generally observed. Recently, Hsu *et al.* (31) synthesized sulfated zirconia that was promoted with iron and manganese and this catalyst was found to be very active for *n*-butane isomerization at 300 K. We (32) have been able to verify that sulfated zirconia promoted with iron and manganese is capable of isomerizing *n*-butane at near room temperature with rates approximately two to three orders of magnitude greater than sulfated zirconia as claimed by Hsu *et al.*

Lin and Hsu (33) conducted a series of temperature-programmed desorption (TPD) experiments on sulfated zirconia in the absence and presence of Fe and Mn. Alkyl and fluorobenzenes of different basicities were used as adsorbates to differentiate between the acidity of these two materials. The adsorptions of fluorobenzenes were found only on the promoted catalyst and thus, Lin and Hsu claimed that the promoted zirconia had much stronger acid sites than those found in sulfated zirconia. Furthermore, they demonstrated that the promoted catalyst contained a greater number of acid sites than the unpromoted catalyst by comparing the TPD peak areas of the desorbed

[1] To whom correspondence should be addressed.

0021-9517/96 $12.00

alkylbenzenes between the two solids. In our previous TPD study on the promoted catalyst (32), we did not observe any correlation between the TPD peak area (from benzene) at 560°C and the *n*-butane isomerization activity as suggested by Lin and Hsu (33), and we found that the TPD peaks originated from CO_2, SO_2, and trace of O_2, indicating the adsorbed benzene was totally oxidized.

Recent Fourier transform infrared (FTIR) and nuclear magnetic resonance (NMR) studies by Adeeva *et al.* (25) suggest that the Brønsted and Lewis acid strengths of surface sites on iron- and manganese-promoted sulfate zirconia are similar to those of the unpromoted sulfated zirconia. Additionally, the Brønsted acid strength does not appear to exceed that of Zeolite HY. Gates and co-workers have also found no evidence in the high-temperature cracking of pentane and butane for any extraordinary acid strength on the promoted sulfated zirconia as compared to sulfated zirconia and zeolites (26, 27). Hence, it is now speculated that both the promoted and unpromoted sulfated zirconia catalysts are not superacidic (25–28). In addition, Tábora and Davis (28) report that the IR spectra from surface sulfate groups, adsorbed pyridine, and adsorbed CO were minimally affected by the promoters with sulfate zirconia and concluded that Fe and Mn do not alter the surface properties of the oxide or substitute into the tetragonal Zr structure (shown by EXAFS of Zr and Fe). Thus, at this time, the origin of high activity for *n*-butane isomerization of the promoted sulfated zirconia remains unknown. The objective of this work is to investigate the nature of the active site for *n*-butane isomerization over Fe- and Mn-promoted sulfated zirconia.

EXPERIMENTAL

1. Catalyst Preparations and Characterizations

The iron- and manganese-promoted samples were prepared from $Zr(OH)_4$ (Magnesium Elektron, Inc., 15 μm) by stepwise impregnation. Three solutions, 0.15 *M* $Mn(NO_3)_2$, 0.30 *M* $Fe(NO_3)_3$, and 3 wt% SO_4^{2-} were prepared by dissolving the appropriate amounts of $Mn(NO_3)_2 \cdot 9H_2O$, $Fe(NO_3)_3 \cdot 6H_2O$, and $(NH_4)_2SO_4$ (all purchased from Aldrich) in deionized, doubly distilled water. Manganese, iron, and sulfate were impregnated one at a time onto the dried $Zr(OH)_4$ by mixing with a 1.5-ml solution per gram of $Zr(OH)_4$. The mixture was stirred for 15 min at room temperature and then filtered without washing. After each impregnation, the sample was dried overnight at 150°C in air. All solids used in this work are labeled by their composition (S, sulfate; F, iron; M, manganese; Z, zirconium oxide) with letters in reverse chronological order of impregnation, i.e., SFMZ is zirconium hydroxide impregnated first with manganese, then with iron, and finally with sulfate. The as-made solids (brown in color) were either calcined *in situ* in the reactor in flowing dry air at 650°C for 3 h before reactions or precalcined in static air at 600°C for 3 h and stored in ambient air. The calcined material is gray in color.

X-ray powder diffraction (XRD) patterns were collected on a Scintag XDS-2000 diffractometer that is equipped with a liquid-nitrogen-cooled Germanium solid-state detector using Cu$K\alpha$ radiation. *In situ* diffuse reflectance fourier transform infrared spectra were obtained on a Nicolet FTIR 800 spectrometer using a Spectra-Tech environmental cell. Each absorption spectrum reported is the average of 1000 scans. All spectra were recorded at either 30 or 100°C after *in situ* heating to a given temperature. Thermogravimetric analyses (TGA) were performed in air at a heating rate of 5°C/min on a DuPont 951 thermogravimetric analyzer. BET surface areas were measured by adsorption of N_2 at −196°C using an Omnisorp 100 analyzer (Coulter). Elemental analyses were performed by Galbraith Laboratories (Knoxville, TN). Scanning electron micrographs were recorded on a CamScan Series 2-LV SEM. EDAX analyses were performed with a Tracor Northern 5500 EDS system.

2. Reaction Studies

Isomerizations of *n*-butane to isobutane were carried out in a single downward flow, fixed-bed reactor at 30 and 100°C, under ambient pressure. Either 0.5 g of the as-made sample was calcined (650°C, 3 h) and cooled under dry air flow (50 ml/min) in the reactor or the precalcined sample was preheated (250–650°C, 1.5 h in air or helium at 50 ml/min) *in situ* in the reactor and cooled to the reaction temperature under the same heating gas. The calcined samples were purged with helium (50 ml/min) at room temperature or 100°C for at least 15 min before being exposed to a mixture of 20% *n*-butane in helium (Matheson) flowing at 5 ml/min. All gases were vigorously dried. The product gases were analyzed using an on-line HP 5890 series II gas chromatograph equipped with a 50 m HP-1 cross-linked methyl-silicone gum column and a flame ionization detector.

3. Temperature-Programmed Desorption Studies

Temperature programmed desorption experiments were conducted in a single downward-flow, fixed-bed reactor at ambient pressure. The as-made sample, 0.3 g, was calcined to 650°C and cooled *in situ* to adsorption temperature (T_{ads}) under dry air flow. T_{ads} was set at 20°C above the bp of the adsorbate. Upon cooling, the sample was exposed to a flow of helium (200 ml/min), after which 30–100 μl of adsorbate was introduced into the helium stream through a septum. The dry helium flow was continued for an additional 30 min to allow removal of any physisorbed adsorbate. Desorption was conducted under the same helium flow by raising the temperature at a rate of 10°C/min to

TABLE 1

Elemental Composition and BET Surface Area of Calcined Materials[a]

Sample	Composition (wt%)			Surface area (m^2/g)
	Sulfur	Iron	Manganese	
SZ	1.2	—	—	125
SFMZ	1.4	1.2	0.9	105

[a] Calcined at 650°C in dry air flow for 3 h and then exposed to ambient conditions prior to analysis.

over 680°C. The desorbed gases were analyzed using an on-line Balzers Quadstar 421 quadrupole gas analyzer. Temperature-programmed oxidation experiments were conducted after the TPD run by heating the sample in a dry air flow at a heating rate of 10°C/min to over 700°C. *p*-Xylene, toluene, benzene, perfluorobenzene, and isopropylamine were used as adsorbates. Carbon monoxide (1% in helium) adsorption/reaction at room temperature was performed in a similar manner.

RESULTS AND DISCUSSION

1. Catalyst Preparations and Characterizations

The elemental compositions and BET surface areas of the calcined materials (650°C in dry air flow for 3 h) are listed in Table 1. The elemental compositions shown here are typical of those reported in the literature (25, 28, 31, 33). All SFMZ samples turn gray after calcination in air to over 600°C and show an XRD pattern indicative of tetragonal zirconia. Typical weight lost upon calcination to 650°C in air is about 21% (from TGA), and no sulfate decomposition is detected. When heated above 690°C, SO_2, and O_2 are released through the decomposition of sulfate. SEM photographs of samples prepared by different methods show different morphologies. For the SFMZ sample prepared by direct impregnation of Fe and Mn onto hydrated zirconium oxide that was obtained from the precipitation of $ZrOCl_2 \cdot 8H_2O$ (described in Ref. (32)), large particles of iron and manganese oxides are found on the surface of the zirconia (Fig. 1). Figure 2 shows SFMZ sample prepared from the coprecipitation of Fe and Mn oxides from a homogeneous solution of Fe and Mn precursors (described by Hsu *et al*. (31)) and a sample prepared from impregnation of Fe and Mn onto dried $Zr(OH)_4$ (described in the experimental section and used here for catalytic studies). Both samples reveal uniform distributions of iron and manganese, as shown by the EDAX mappings of the coprecipitated sample in Fig. 3. Similar EDAX mappings are found for the sample prepared from impregnation of Fe and Mn onto dried $Zr(OH)_4$ (not shown). Interestingly, all of these samples are very active for the near room-temperature isomerization of *n*-butane suggesting that only a very small percentage of the promoting metals is involved in the active site. Tábora and Davis (28) showed by EXAFS experiments that Fe does not substitute directly for Zr and they concluded also that only a small portion of Fe/Mn plays a role in the *n*-butane isomerization catalysis.

Figure 4a shows the FTIR spectra from SZ and SFMZ before and after adsorption of pyridine at 100°C. Pyridine adsorption has been known to be able to distinguish between Brønsted and Lewis acid sites (34–36). The characteristic bands of the pyridinium ion at 1640, 1610, 1542, and 1490 cm^{-1} are observed and indicate the presence of Brønsted acidity on both solids. Additionally, bands at 1607, 1575, 1490, and 1445 cm^{-1}, which correspond to pyridine adsorbed on Lewis acid sites, are observed on SZ and SFMZ. Quantitative number densities of the various adsorption complexes from IR spectra are difficult to obtain. Thus, only the ratios of the Brønsted acid to the Lewis acid sites are calculated and they are 0.5 and 1.0 for SZ and SFMZ, respectively. The ratios obtained here are exactly the values reported by Tábora and Davis (28). Since the amount of Brønsted acid sites tends to increase with increasing overall sulfate loadings, as recently suggested by Nascimento *et al*. (37), the different Brønsted to Lewis ratios (B/L) found in SZ and SFMZ are probably due to different sulfate loadings per surface area (see Table 1). Nascimento *et al*. (37) also reported a sulfated zirconia with a B/L ratio of one. As a result, the difference in the B/L ratio found for SZ and SFMZ is unlikely to be responsible for a two orders of magnitude difference observed in catalytic activity of SZ and SFMZ (28, 31, 32). The adsorption of pyridine was conducted after various stages of the *n*-butane reaction and the FTIR spectrum recorded (Fig. 4b). Also, *in situ* FTIR spectra of SZ and SFMZ were obtained at various stages of the reaction, as shown in Figs. 5 and 6. Spectra were taken at 1 and 2 h after the commencement of the reaction, at which time the catalyst was still active. Additionally, spectra of the as-made, the freshly calcined, and the deactivated (10 h on stream) samples were also recorded. It is again clear from these data that no significant changes are found throughout the reaction profile for both catalyst systems. Similarly, no difference is found in the IR spectrum of adsorbed pyridine from the SFMZ sample that had been subjected to vacuum treatment at room temperature (Fig. 7). Interestingly, SFMZ samples pretreated under vacuum at room temperature after calcination in air are all found to be less active than those not exposed to vacuum. Details of the vacuum treatment on *n*-butane isomerization activity are presented below.

On the basis of the above findings, we speculate that two possible scenarios exist. First, the active site number

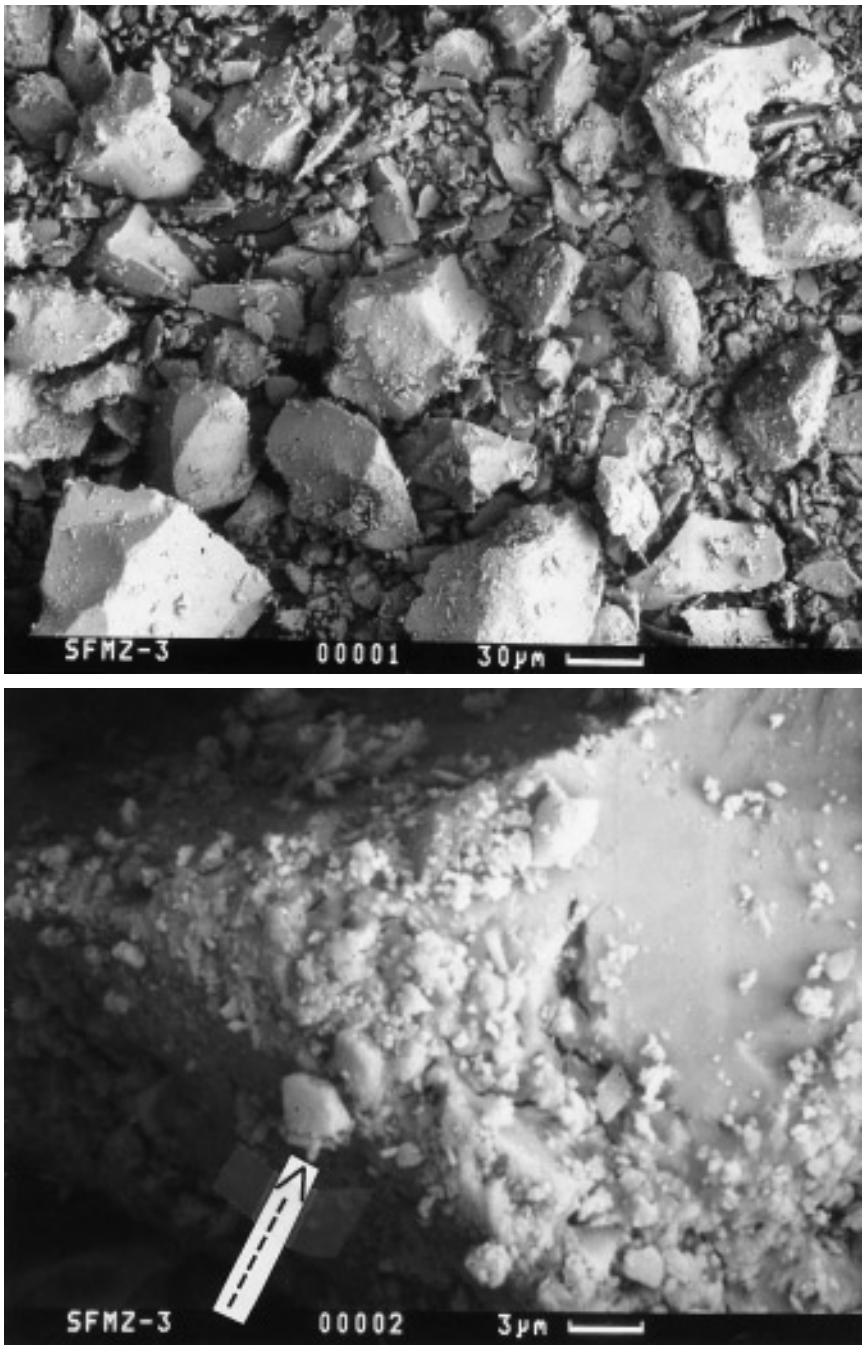

FIG. 1. SEM photographs of SFMZ samples prepared by impregnation of Fe and Mn onto hydrated zirconia oxide prepared from $ZrOCl_2 \cdot 8H_2O$. Arrow points to a 3-μm area of concentrated iron oxide.

density may be very small. Second, the *n*-butane isomerization involves more than one active site, and the spectroscopic characterizations are not probing the combination of active sites necessary for reaction. These points are addressed below.

2. Reaction Studies

Typical time-dependent *n*-butane conversion data at 30 and 100°C are shown in Fig. 8. The extraordinary activity of the iron- and manganese-promoted sulfated zirconia for low-temperature isomerization of *n*-butane is again confirmed. Upon deactivation of the catalyst, regeneration is possible only by calcination in air (not in helium). The conversion profile at 30°C is characterized by two distinct regimes: a break-in period followed by a slow deactivation period. In contrast, at 100°C, no maximum in conversion is observed. Because of the lag time between the reactor and GC, samples taken at times less than 17 min are likely

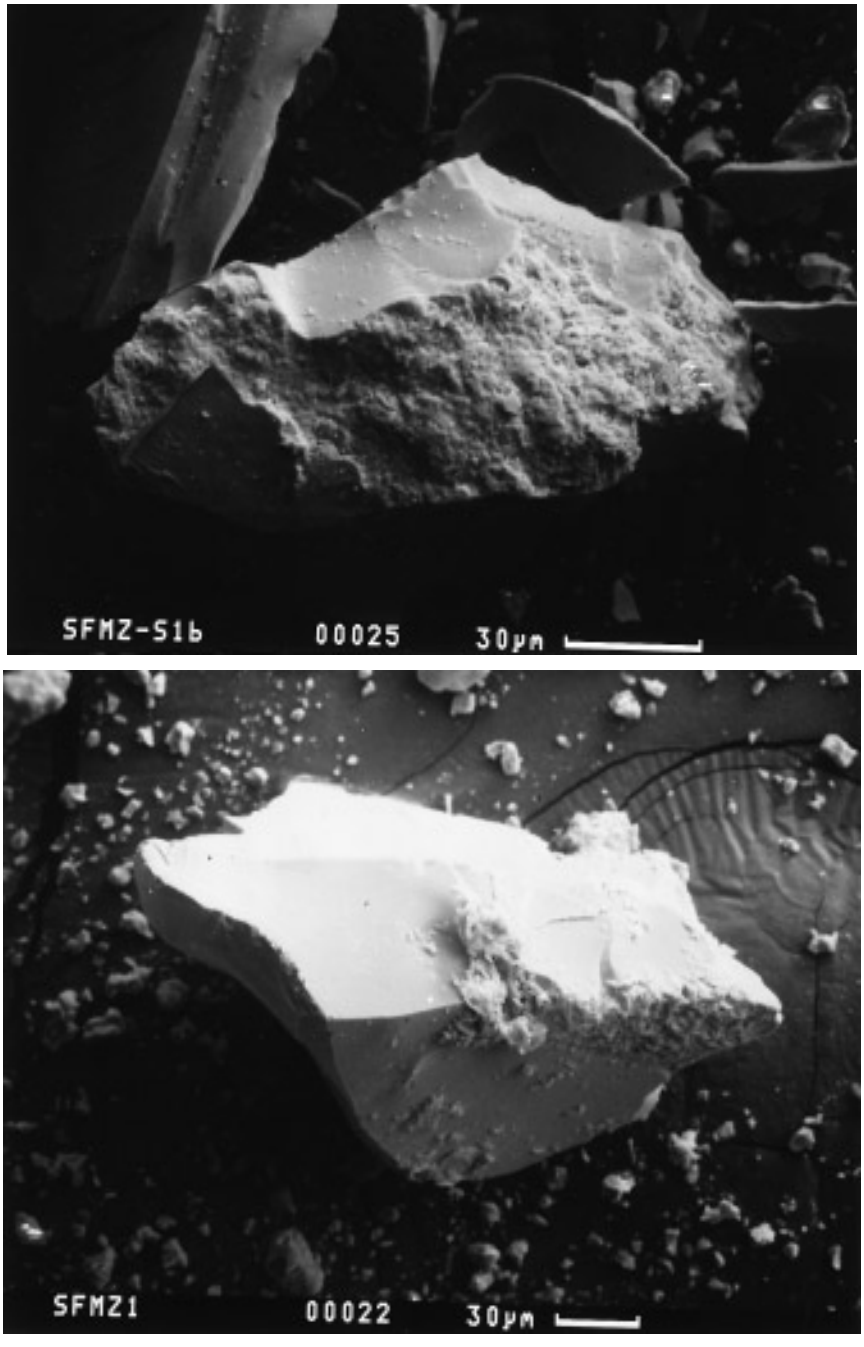

FIG. 2. SEM photographs of SFMZ samples. Top, prepared by precipitation; bottom, prepared by impregnation.

to be influenced by incomplete removal of the helium in the reactor system prior to the introduction of the *n*-butane feed. Thus, it is highly possible that a maximum in conversion may have occurred at times less than 17 min on stream. However, it is quite clear that the catalyst deactivates more rapidly at 100°C than at 30°C. Reaction rates are calculated from conversion data collected during the period of near maximum conversions. An apparent activation energy of 10.5 kcal/mol for the near room-temperature *n*-butane isomerization is determined from an Arrhenius plot of our data over the temperature range 30–55°C. Hsu *et al.* (31) reported the apparent activation energies of 11.4 and 10.7 kcal/mol for SFMZ and SZ, respectively, and suggested that the improvement in activity represented by the promoted catalyst is associated with a larger number of catalytic sites than in sulfated zirconia.

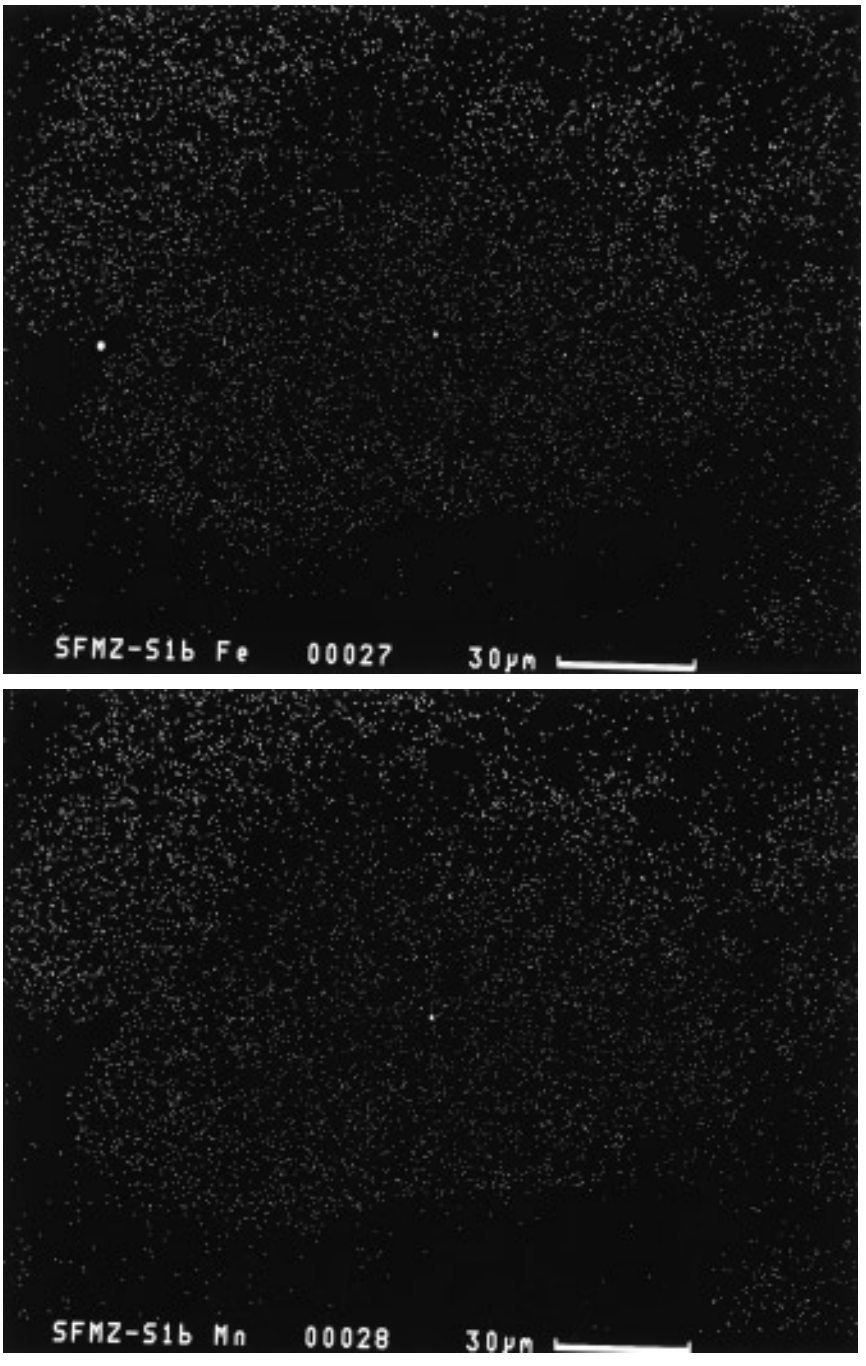

FIG. 3. EDAX mappings of Fe and Mn in SFMZ sample prepared by coprecipitation.

We initiated our catalytic studies with as-made materials. Samples were calcined *in situ* to 650°C in dry air flow for 3 h before reaction. As shown in Table 2, entries 1–4, four different batches of samples were tested and found to give similar conversions, i.e., 10–12%. The activities obtained here are typical of those reported by Tábora and Davis (28) and Hsu *et al.* (31). When using samples that have been precalcined at 600°C in static air for 3 h (entries 5–8 in Table 2), higher conversions (16–19%) are always obtained under the same conditions due to the 21% weight lost upon initial calcination (from nitrate decomposition, water loss, etc.). As the precalcined sample has already crystallized to the tetragonal phase during the initial calcination, it is a good starting material to study the effect of pretreatment conditions on the catalytic activity (and is used in most of the catalytic studies reported below).

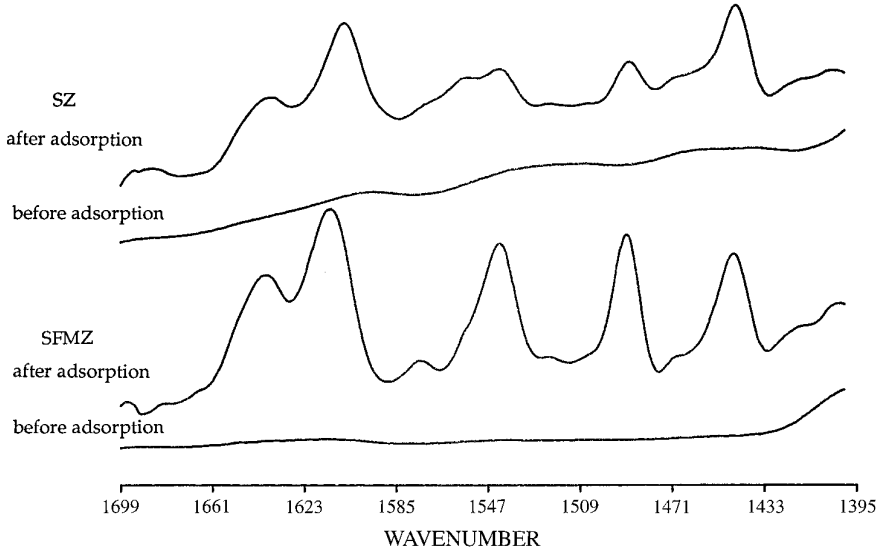

FIG. 4a. IR spectra of adsorbed pyridine on SZ and SFMZ.

In our previous work (32), we showed that the addition of manganese is not mandatory for *n*-butane isomerization activity at 30°C. Thus, in our discussion below we address the role of iron and suppose that analogous behavior may occur with manganese. As evidenced by the data in Table entries 6 and 9, it is important to note that calcination in the presence of oxygen is required for high activity at 30°C; only 0.4% conversion is observed when the sample is calcined in helium (entry 9). By further calcining the catalyst treated with He in air to 650°C, the activity (17.1% vs 18.7%) is recovered (entry 10). Also, when an as-made sample is calcined in air and then recalcined *in situ* in helium to 650°C for 3 h, the material is again found to be inactive for the isomerization of *n*-butane at 30°C (entry 11). Hence, it is apparent that the calcination in helium reversibly inhibits *n*-butane isomerization activity at 30°C. In addition to the instability of the active site toward helium exposure at 650°C, the catalyst is affected by vacuum

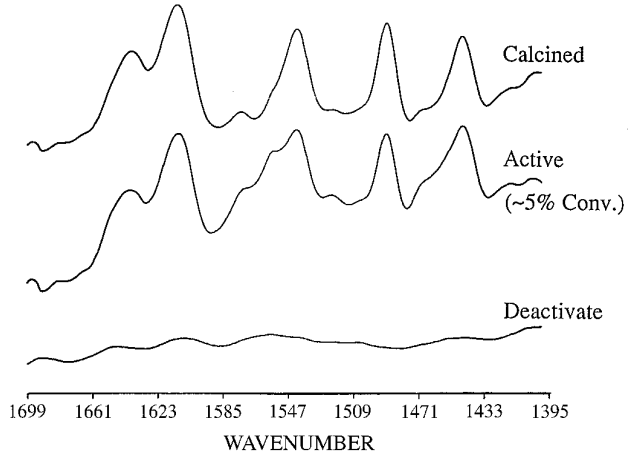

FIG. 4b. *In situ* IR spectra of adsorbed pyridine on SFMZ at various stages of reaction.

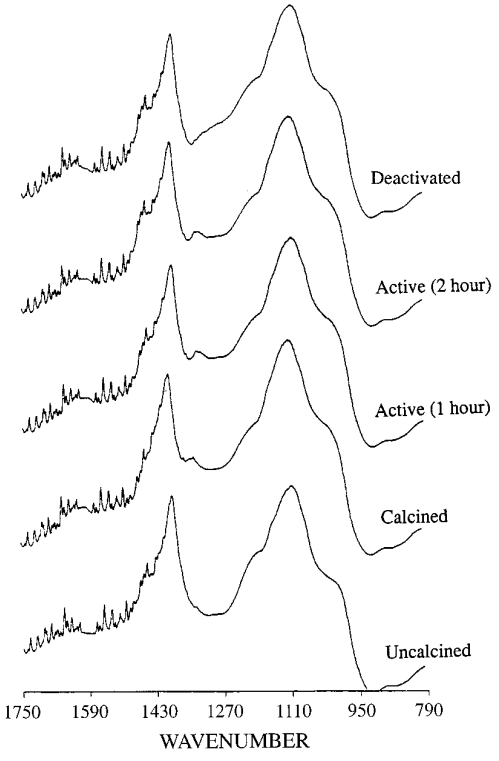

FIG. 5. *In situ* IR spectra of SZ at various stages of reaction.

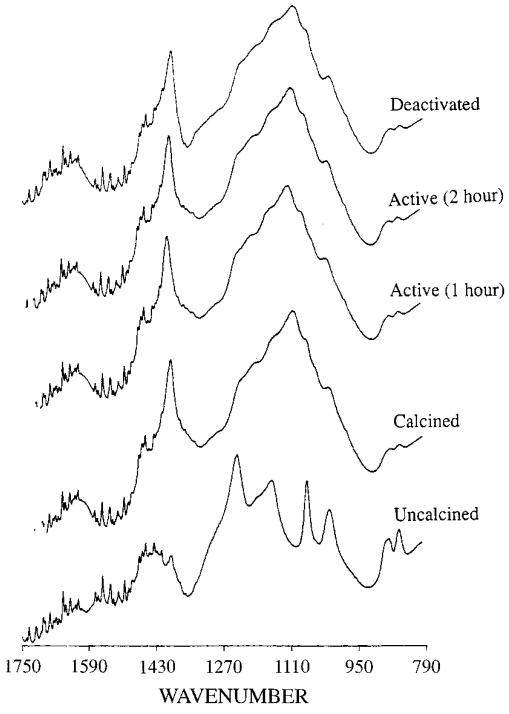

FIG. 6. *In situ* IR spectra of SFMZ at various stages of reaction.

(entries 12 and 13). These results show that a rather labile active site is responsible for the near room-temperature isomerization of *n*-butane. The requirement of oxygen for the activation of the catalyst suggests the presence of a metal oxy species necessary for reaction at 30°C. The instability of this species toward vacuum treatment at room temperature suggests that it involves a relatively labile oxygen. To further justify this assumption, recalcination of the solid in pure hydrogen to 400 or 650°C results in a

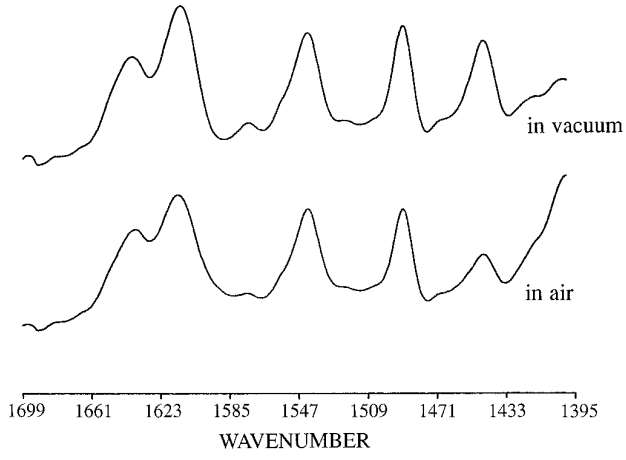

FIG. 7. IR spectra of adsorbed pyridine on SFMZ that was pretreated in vacuum and air.

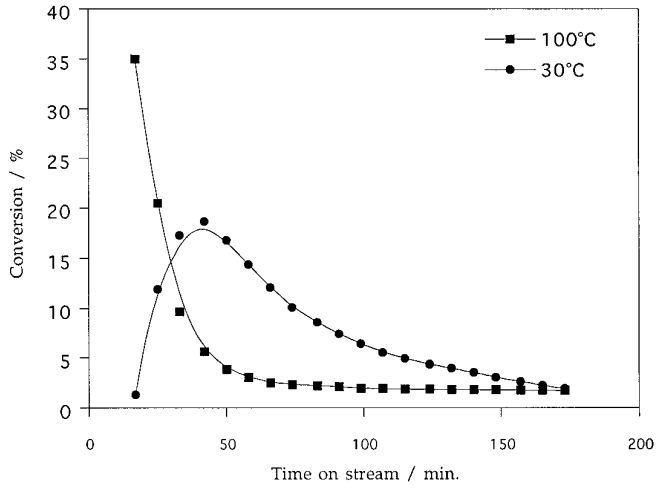

FIG. 8. Typical reaction profile for the *n*-butane isomerization by SFMZ at 30 and 100°C.

lack of *n*-butane activity even after subsequent calcination in air (entries 14 and 15). It is possible that calcination of the solid in hydrogen reduces surface iron oxides to metallic clusters which are difficult to reoxidized by calcination in air. It is also likely with the exposure to hydrogen at 650°C (but not 400°C) that the loss in catalytic activity is through the loss of acid sites via the decomposition of sulfate. Hence, in contrast to helium treatment, calcination in hydrogen irreversibly destroys the catalyst.

These results are not consistent with the idea that superacidity is responsible for *n*-butane isomerization activities at 30°C. The catalytic data presented above appear to rule out the possibility of an iron-/manganese-induced superacid site in the SFMZ catalyst because an acid center should not be unstable to vacuum. Instead, we believe the high-temperature air calcination generates a rather labile but reactive oxy species that is not stable toward either room-temperature vacuum treatment or high-temperature recalcination in helium. Such oxy species could play a crucial role in providing for the near room-temperature pathway to the formation of isobutane through an initial oxidative dehydrogenation of *n*-butane to butene (followed by acid-catalyzed coupling and rearrangement on the acid sites). Details of our proposed mechanism are discussed below.

Cheung *et al.* (38) used a precalcined sample of SFMZ (500°C in static air for 3 h) for the isomerization of *n*-butane at 40°C. After preheating to 450°C for 1.5 h in nitrogen, they report a 6% (after 4 h on stream) conversion at 40°C. Under the same pretreatment conditions, they also show over 40% conversion at 100°C. Hence, at first glance, it appears that our proposed formation of an active oxy species by a necessary high-temperature air calcination is inconsistent with the results presented by Cheung *et al.*

TABLE 2

Catalytic Data of *n*-Butane Isomerization by SFMZ at 30°C

Entry	Pretreatment conditions	Activation	Reaction temp. (°C)	Maximum conv. (%)	Maximum rate (mol/(g of cat. s))	Time to max. conv. (min.)
1	As-made	Calc. in air at 650°C for 3 h	30	11.5	1.55E-07	66
2	As-made	Calc. in air at 650°C for 3 h	30	11.9	1.60E-07	52
3	As-made	Calc. in air at 650°C for 3 h	30	9.9	1.33E-07	82
4	As-made	Calc. in air at 650°C for 3 h	30	11.3	1.52E-07	66
5	Precalcined	Calc. in air at 650°C for 3 h	30	16.5	2.21E-07	74
6	Precalcined	Calc. in air at 650°C for 3 h	30	18.7	2.51E-07	41
7	Precalcined	Calc. in air at 650°C for 3 h	30	12.8	1.72E-07	66
8	Precalcined	Calc. in air at 650°C for 3 h	30	15	2.01E-07	66
9	Precalcined	Calc. in helium at 650°C for 3 h	30	0.4	5.36E-09	237
10	From entry 9	Calc. in air at 650°C for 3 h	30	17.1	2.29E-07	41
11	Precalcined	Calc. in air at 650°C for 3 h, then recalc. *in situ* in helium at 650°C for 3 h	30	0.3	4.02E-09	237
12	Precalcined	Calc. in air at 650°C for 3 h, then vacuum at 30°C for 1 h	30	9.2	1.23E-07	66
13	Precalcined	Vacuum at 30°C for 3 h	30	7.7	1.03E-07	58
14	Precalcined	Calc. in hydrogen at 650°C for 3 h	30	0	0	—
15	From entry 14	Calc. in air at 650°C for 3 h	30	0	0	—
16	Precalcined	Calc. in helium at 450°C for 3 h	30	2.9	3.89E-08	277

(38) who employed calcination in an inert atmosphere. To clarify this inconsistency, precalcined materials (600°C in static air for 3 h) were activated at the pretreatment conditions reported by Cheung *et al*. (38), i.e., preheated at 450°C for 1.5 h in helium, then reaction at 100°C. As shown in Table 3 entry 5, a 27.3% conversion is observed. For comparison, a 28.9% (entry 6) conversion is obtained when the sample is preheated in dry air before reaction. It is therefore apparent that under the present pretreatment conditions, the type of calcination environment (air or helium) has no effect on activities at 100°C. To further test this effect, a series of reactions were conducted at 100°C in order to study the relationship between pretreatment conditions and *n*-butane isomerization activity. As listed in Table 3 entries 1–6, similar conversions are found with either helium or air in the calcination environment at temperatures below 450°C. However, when the preheating temperature is increased to above 450°C, the activity of the sample preheated in helium deviates from the one preheated in air. At a preheating temperature of 550°C,

TABLE 3

Catalytic Data of *n*-Butane Isomerization by SFMZ at 100°C

Entry	Activation (all precalcined)	Reaction temp. (°C)	Maximum conv. (%)	Maximum rate (mol/(g of cat. s))	Time to max. conv. (min.)
1	Calc. in helium at 250°C for 1.5 h	100	25.3	2.76E-07	17
2	Calc. in air at 250°C for 1.5 h	100	23.1	2.52E-07	17
3	Calc. in helium at 350°C for 1.5 h	100	35	3.81E-07	17
4	Calc. in air at 350°C for 1.5 h	100	32.6	3.55E-07	17
5	Calc. in helium at 450°C for 1.5 h	100	27.3	2.97E-07	17
6	Calc. in air at 450°C for 1.5 h	100	28.9	3.15E-07	17
7	Calc. in helium at 550°C for 1.5 h	100	22.2	2.42E-07	25
8	Calc. in air at 550°C for 1.5 h	100	34	3.70E-07	25
9	Calc. in helium at 650°C for 1.5 h	100	15.4	1.68E-07	25
10	Calc. in air at 650°C for 1.5 h	100	37.1	4.04E-07	17
11	Calc. in helium at 350°C for 1.5 h, then vacuum at 30°C for 1 h	100	33.1	3.61E-07	17
12	Calc. in air at 350°C for 1.5 h, then vacuum at 30°C for 1 h	100	30.4	3.31E-07	17

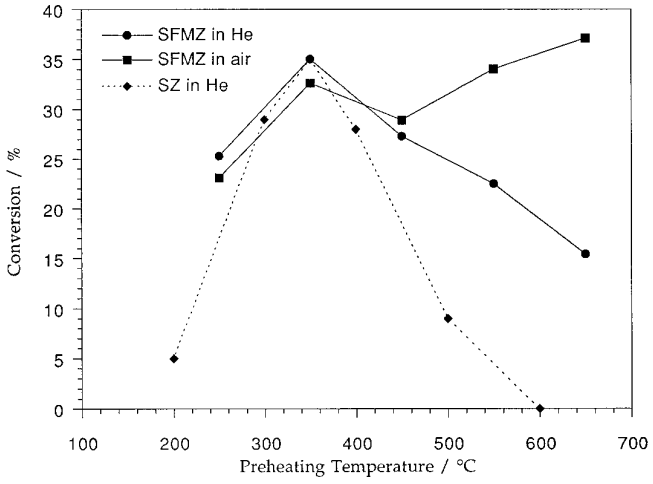

FIG. 9. Effects of preheating conditions on activity at 100°C.

the sample preheated in dry air is more active than that in helium (34.0% vs 22.5%, entries 8 and 7 in Table 3). The difference is even larger when the preheating temperature is 650°C: 37.1% with air versus 15.4% with helium (entries 10 and 9 in Table 3). Figure 9 shows the conversion as a function of the preheating temperature. For the case of samples preheated in helium, a maximum in the conversion is observed at a preheating temperature of 350°C. The catalytic behavior of SFMZ at 100°C for samples preheated in helium is compared to that of sulfated zirconia (shown as dotted line in Fig. 9) (22). A bell-shaped relationship between conversion and preheating temperature is found for both these two materials. Maximum conversions are observed at a 350°C preheating temperature. For sulfated zirconia, the activity is more sensitive to the preheating temperature. Arata (22) proposed that residual moisture on the catalyst is important for reactivity and suggested that the Brønsted acid sites are necessary for activity with SZ. Thus, SZ samples from high-temperature calcinations that lead to the removal of Brønsted acid sites are not active. However, our findings of relatively long-lived activities with 15–22% conversion (entries 7 and 9 in Table 3) at preheating temperatures of 550–650°C in helium clearly suggests that the catalytic behavior of SFMZ at 100°C is different from that of SZ. With the SFMZ samples preheated in air, two different types of catalytic behavior are apparent. Below a preheating temperature of 450°C, the catalytic behavior is nearly the same as that from the material preheated in helium. Above 450°C, the samples calcined in air are much more active than those preheated in helium.

On the basis of these results, we propose a ''three-site'' model for *n*-butane isomerization. The first site requires high-temperature (>450°C) calcination in air, while the other two can be generated in its absence. We suggest that an oxy species is an active site generated by high-temperature calcination in air (above 450°C) and that it is very active for *n*-butane isomerization at 30 and 100°C. The second site is also active at 100°C and diminishes in activity as the reaction temperature is lowered. The formation of this site in the absence of air suggests that it could be an iron (III) species, which already exists in the precalcined material and will not be reduced by thermal treatment in helium. Either of these two metal sites must be accompanied by a third site, an acid site, in order to be active for *n*-butane isomerization. This remaining acid site is present in both SZ and SFMZ. The three-site model can also explain why samples calcined in air are more active than those reported by Cheung *et al.* (38), e.g., 18.7% vs 6% in the above room-temperature isomerization of *n*-butane. In contrast to the proposed oxy species that has been shown to be rather labile, the presumed iron (III) species is stable toward vacuum treatment at room temperature (33.1% vs 35.0% preheated in helium and 30.4% vs 32.6% preheated in air, entries 11 and 12 in Table 3), indicating that it is indeed different from the oxy species that is proposed to be responsible for activities at 30°C. The onset of reactivity on SFMZ from this iron (III) species (2.9% vs 27.3%, entry 16 in Table 2 and entry 5 in Table 3) is likely to be due to the increase in the reaction temperature from 30 to 100°C. Hence, it is important to note that different active species can be generated under different preheating conditions. Additionally, the results shown in Fig. 9 provide additional strong evidence against the postulation that superacidity contributes to the activity in the near room-temperature isomerization of *n*-butane because of the observed dramatic difference in catalytic behavior between preheating in air and helium at above 450°C.

Pinna *et al.* (39) reported that the *n*-butane isomerization activity of sulfated zirconia at 150°C was reversibly suppressed by addition of carbon monoxide and concluded that Lewis acid sites were important for activity. With SFMZ, a poisoning effect of carbon monoxide on the near room-temperature activity is observed. The entire reaction profile of our carbon monoxide poisoning experiment is shown in Fig. 10. The catalyst is activated *in situ* to 650°C in air, and then *n*-butane isomerization is conducted at 30°C. Pure carbon monoxide (1 ml/min) is introduced into the *n*-butane feed while the conversion is still increasing. Within minutes, the activity declined to zero and was not recovered even after heating to 200°C in helium (used to remove CO from any Lewis acid sites). For sulfated zirconia, the original activity is completely recovered upon removal of carbon monoxide at a reaction temperature of 150°C (39). By increasing the reaction temperature to 200°C, the CO-poisoned SFMZ catalyst becomes active. As expected, the catalyst deactivated rapidly within hours. The near room-temperature activity could only be recovered by recalcination in air to 650°C. These findings suggest

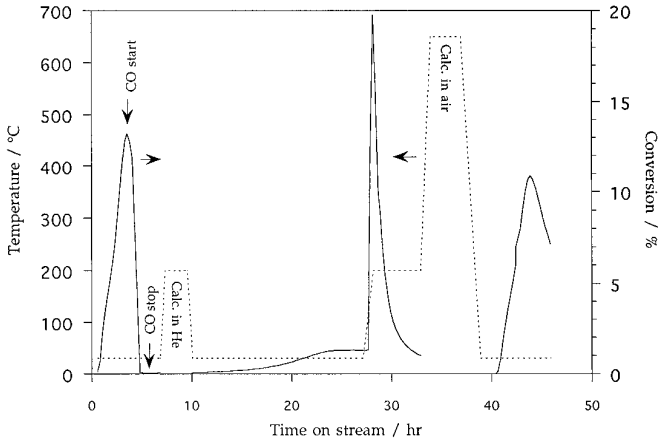

FIG. 10. Reaction profile for the CO poisoning experiment on SFMZ.

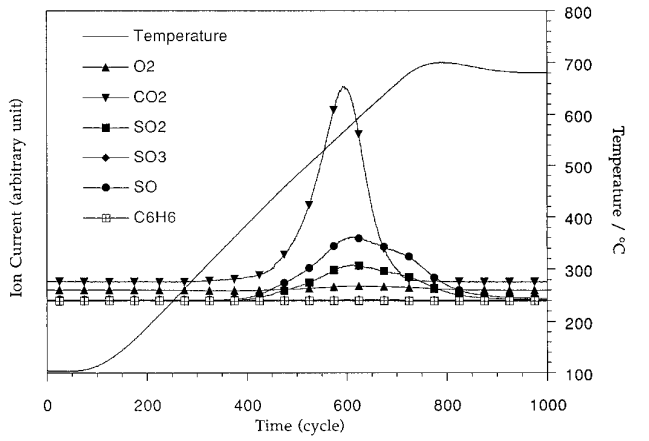

FIG. 12. Benzene TPD profile of SFMZ.

that the proposed oxy species are affected by the carbon monoxide treatment at 30°C, while other sites, e.g., iron (III) species and/or Brønsted/Lewis acid sites, are still active at 200°C. The air recalcination necessary to recover the 30°C activity is a strong indication that the oxy species are poisoned by carbon monoxide. To understand the mechanism of carbon monoxide poisoning in SFMZ, reaction products from carbon monoxide exposure are monitored with an on-line mass spectrometer. Spontaneous evolution of carbon dioxide is observed upon the introduction of carbon monoxide to SFMZ at 30°C (Fig. 11). No traces of sulfate reduction are found as shown by the lack of SO and SO_2 evolution. Furthermore, no carbon residue (from CO disproportionation) is found on the surface after the CO experiment (ascertained by a subsequent temperature-programmed oxidation (TPO) step). When the carbon monoxide poisoning experiment is conducted with a SFMZ sample that has been calcined *in situ* in helium to 650°C, no carbon dioxide is detected. Since the *in situ* calcination in helium has been shown to reversibly inhibit the *n*-butane isomerization activity at 30°C, the above findings suggests that carbon monoxide selectively poisons the active site responsible for *n*-butane isomerization at 30°C (if the He-treated sample is calcined in air, room-temperature CO reactivity returns). We therefore conclude that carbon monoxide is oxidized to carbon dioxide by the oxy species at 30°C. More importantly, the carbon monoxide reaction provides a direct way to selectively study the number density of the oxy site at near room-temperature conditions. Assuming a stoichiometry of one CO reacting to one CO_2 with one oxy site, the CO is reacted until no further CO_2 evolution is detected and the cumulative amount of CO_2 recorded. Using this approach, the number density of this oxy species is determined to be 10–15 μmol/g of catalyst, i.e., 0.10–0.14 μmol/m^2. We speculate that this oxy species is responsible for the oxidative dehydrogenation of *n*-butane to butene, which then forms a C_8 intermediate to ultimately give isobutane. No trace of butene was detected during the reaction. However, a very small amount of butene could account for the 30°C *n*-butane isomerization activity since it has already been shown that there is sensitive dependence of the acid-catalyzed cracking of *n*-butane on traces (below detectable amounts) of olefinic initiators (40).

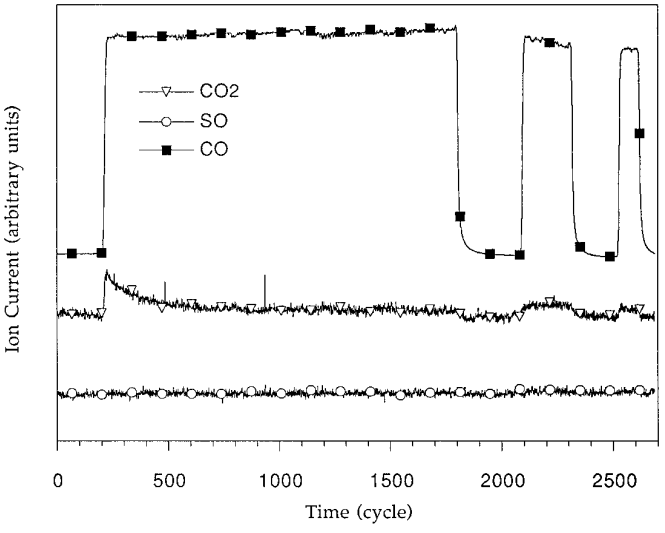

FIG. 11. MS profile from the CO poisoning experiment on SFMZ at 30°C (1% CO in He at 150 ml/min).

3. Temperature-Programmed Desorption Studies

The benzene TPD profile from SFMZ is shown in Fig. 12. As indicated in our previous paper (32), no high-temperature benzene desorption is found. Instead, desorptions of CO_2 and SO_2 at 560–580°C are observed. For sulfated zirconia, no high-temperature desorption of any kind of

carbon-containing species is observed, and the surface is completely carbon free after the TPD run (not shown). Since CO_2 desorption is not found in samples not exposed to benzene, it is clear that the CO_2 originates from the oxidation of benzene. As SFMZ is stable up to 670°C in helium (no loss of sulfur-containing species), the oxidation of benzene at 565°C cannot be attributed to oxidation by SO_3 generated through the decomposition of sulfate. Lin and Hsu (33) claim that the peak at ~565°C is a consequence of superacid sites capable of adsorbing a weak base, e.g., benzene. However, superacidity if it exists in SFMZ cannot explain the evolution of SO_2 and CO_2. On the basis of our proposed redox-active iron/manganese species, we believe the adsorbed benzene is oxidized by iron/manganese species at the high desorption temperature. To clarify the origin of SO_2, calcinations of iron (II) and iron (III) sulfates were conducted in helium. Iron (III) sulfate is stable up to 670–680°C in helium and decomposes to form O_2, CO_2, and SO_2. In contrast, iron (II) sulfate is relatively less stable and decomposes at 560°C. It also releases far less O_2 than iron (III) sulfate because of its *in situ* oxidation back to iron (III). Hence, the decomposition temperature and the relative amount of O_2 liberated are good indicators of the oxidation state of the iron species involved in the sulfate decomposition process.

The release of only a small amount of oxygen in the benzene TPD of SFMZ at a relatively low desorption temperature (565°C) clearly suggests that the sulfate decomposition originates from a reduced iron species. The mechanism of the conversion of benzene to CO_2 is then rationalized as an oxidation of benzene by the oxy species and/or the iron (III) species, leading to the formation of iron (II), followed by immediate sulfate decomposition at 565°C. This sequence of events can explain the spontaneous evolution of SO_2 with CO_2. To distinguish whether the oxy species or the iron (III) species is responsible for the oxidation of benzene, the benzene TPD experiment is repeated with a SFMZ sample that has been calcined *in situ* in helium to 650°C. Such thermal treatment removes the labile oxy species. A similar benzene TPD profile is found but with only one-third of the amount of CO_2 liberated as before. Additionally, a sample of SFMZ heated in helium at 450°C is also able to oxidize benzene. These results suggest that both the iron (III) and the oxy species are capable of oxidizing the adsorbed benzene to carbon dioxide by 565°C. The absence of any desorption peak from sulfated zirconia rules out any redox-active sulfate site. It should be noted that superacidity is not involved in our proposed mechanism for the formation of CO_2 and SO_2. Instead, we believe that the benzene molecule is initially adsorbed onto an Fe and/or Mn site and is subsequently oxidized at high temperature. The exact mechanism of the oxidation process is still unclear at this stage. Although quantitative results from the integration of the

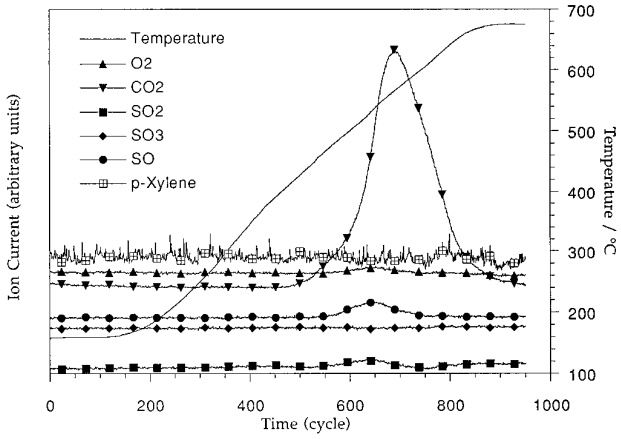

FIG. 13. *p*-Xylene TPD profile of SFMZ.

CO_2 peak area are unreliable due to the carbonaceous residue left behind after the TPD run, estimates based on the relative amounts of CO_2 desorbed indicate an apparent direct correlation between the peak area at 565°C and the catalytic activity for *n*-butane isomerization (as observed by Lin and Hsu (33)), thus further justifying the direct involvement of metal sites in catalytic activity. In our previous results (32), the lack of correlation between the CO_2 peak area and the catalytic activity is likely due to variations in sulfate as well as metal (Fe/Mn) loading. The lack of high temperature CO_2 desorption in the benzene TPD's from $Fe_2(SO_4)_3$, Fe_2O_3 and a physical mixture of $Fe_2(SO_4)_3$/SZ suggest that an intimate coexistence of Fe/Mn and Zr is crucial for the formation of an active Fe/Mn site. A high-temperature CO_2 desorption in the benzene TPD from FMZ rules out the possibility that $FeSO_x$ species are the active sites in the decomposition/desorption mechanism. Lin and Hsu (33) claim the existence of superacid sites that contribute to adsorptions of benzene and even fluorobenzenes in SFMZ. However, with the use of perfluorobenzene under our experimental conditions, both SFMZ and SZ did not show any high-temperature desorption of perfluorobenzene or carbon dioxide. In fact, only decomposition of sulfate at 680°C with liberation of oxygen is observed with SFMZ.

Since SZ does not adsorb benzene, a stronger base was used as the probe molecule to compare the acid strength between the SZ and SFMZ. *p*-Xylene TPD experiments were conducted after adsorption at 160°C. Again, CO_2, SO_2, and a small amount of oxygen are desorbed at around 560°C with SFMZ (Fig. 13). Surprisingly, instead of desorption of intact *p*-xylene, CO_2 and SO_2 are also desorbed from SZ, but at a higher desorption temperature of 610°C (Fig. 14). Similar results are also obtained with toluene on SZ. The shift of the desorption peak to higher temperature suggests that the oxidation mechanism in SZ is different

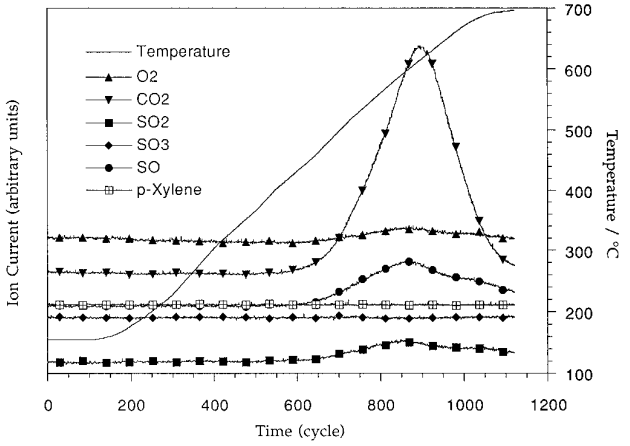

FIG. 14. *p*-Xylene TPD profile of SZ.

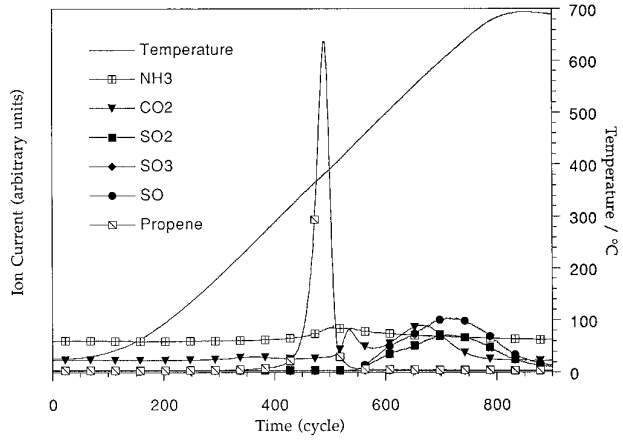

FIG. 15. Isopropylamine TPD profile of SFMZ.

from that in SFMZ and is not unexpected. The oxidation of the adsorbate on SZ could be initiated by a decomposition product of the sulfate.

The unexpectedly high desorption temperature of alkylbenzenes and the absence of any high-temperature benzene desorption on SZ lead us to investigate further the adsorption mechanism of alkylbenzenes. When a *p*-xylene TPD experiment is conducted on $Zr(OH)_4$, no desorption of *p*-xylene or CO_2 is observed. However, CO_2 is released when the sample is reoxidized in air indicating that a carbonaceous residue is formed during the TPD experiment. As *p*-xylene and toluene both contain benzylic hydrogens (which are relatively easy to break), some of the alkylbenzene must be pyrolyzed on zirconia at the adsorption temperature. If such is the case for SZ, the carboneous residue is then oxidized during the high-temperature decomposition of sulfate in SZ. It is therefore quite clear that the desorption channels for the various aromatics on SZ and SFMZ are very different and none of them selectively probe only the acid sites. Therefore in order to number count the Brønsted acid sites, we conducted an isopropylamine TPD experiment. Isopropylamine temperature-programmed desorption experiments have been used to number count the Bronsted sites in silica–alumina and zeolites (41–43). An isopropylamine TPD profile from SFMZ (activated in air to 650°C) is shown in Fig. 15. In addition to propene and ammonia desorptions, CO_2 is also released, again suggesting the oxidation of the probing molecule. The Brønsted acid site density is determined to be 139 μmol/g of catalyst from the desorption of propene fragments [cf. 127 μmol/g reported by Tábora and Davis (28)]. It is noticeable that the CO_2 desorption profile consists of two distinct peaks centered at 420 and 565°C. In the isopropylamine TPD profile of SZ (Fig. 16), only a small peak at 420°C is observed. Thus, the peak at 565°C found only in SFMZ is tentatively assigned as the oxidation product of the probe molecule from the redox-active metal site. When a precalcined SFMZ sample is activated in helium to 650°C, the isopropylamine TPD profile is found identical to the one activated in air. In addition, the release of CO_2 is accompanied by the liberation of SO and SO_2, thus suggesting a redox reaction at the metal site. At this high desorption temperature, it is impossible to differentiate the contributions of the oxy species and the iron (III) species. In fact, it is possible that these two species may originate from the same metal site under different activation conditions. Due to the presence of carbonaceous residue in the post-TPD samples, we are unable to quantify the number density of the redox-active metal sites based on the amount of CO_2 liberated. However, it is quite obvious that the oxidative desorption channel of the probe molecule occurs only on SFMZ.

4. Proposed Mechanism

Results from both the catalytic and the TPD studies suggest the presence of redox-active metal sites. The car-

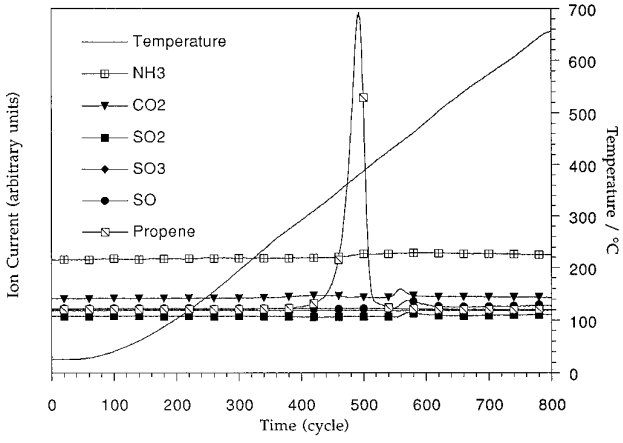

FIG. 16. Isopropylamine TPD profile of SZ.

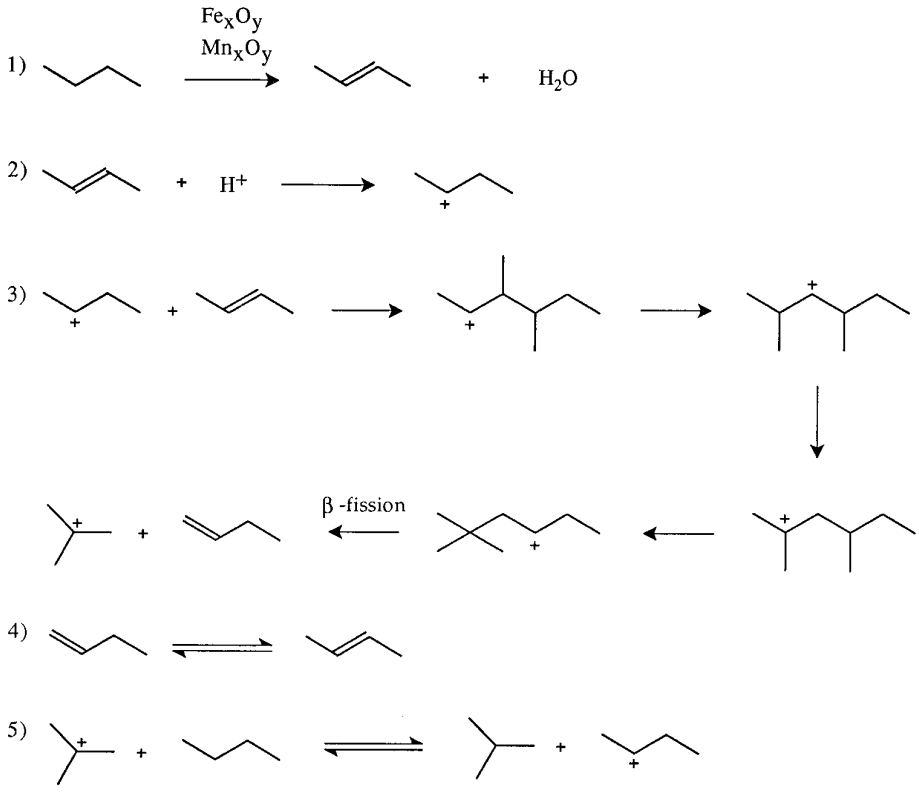

SCHEME 1

bon monoxide poisoning experiment gives additional evidence for redox activity at near room-temperature conditions. A bimolecular mechanism for *n*-butane isomerization on SFMZ is found at both 50 and 100°C via ^{13}C labeling of *n*-butane (44), suggesting that the two metal species (generated under different activation conditions) behave similarly in the reaction mechanism although at significantly different temperatures. The involvement of redox-active metal sites can be used to explain a bifunctional mechanism for the *n*-butane isomerization on SFMZ. Scheme 1 shows a simplified, proposed mechanism for *n*-butane isomerization to isobutane on SFMZ. Under our reaction conditions, we speculate that the metal site is responsible for the oxidative dehydrogenation of *n*-butane to butene (step 1), which is then protonated at the acid site, forming a carbenium ion (step 2). The carbenium ion then couples with another butene via a C_8 intermediate and disproportionates to the *tert*-butyl cation and 1-butene through β-fission (step 3). It is clear that other C_3, C_5, C_8, and even higher oligomers could also be formed from the carbenium ion. Recently, Coelho *et al.* (45) have proposed that the high isomerization activity of a nickel-promoted sulfated zirconia catalyst could be explained in terms of a bifunctional mechanism where the metal promoter is responsible for an enhancement in the surface concentration of butenes rather than an enhanced acidity. Bimolecular pathway for the *n*-butane isomerization by SFMZ at 80°C has also been suggested by Adeeva *et al.* (46) from ^{13}C labeling experiments and by Zarkalis *et al.* (47) via kinetics studies. Disproportionation products consistent with a C_8 intermediate are also observed by Gates and coworkers (38, 47). Under the reaction conditions, the 1-butene can isomerize to the more stable 2-butene and the reaction cycle continues (steps 2 through 4). Note that superacidity is not necessary for this reaction mechanism to proceed. In contrast, and because of the absence of metal-promoted formation of butene, sulfated zirconia either relies on traces of butene present as impurity in the *n*-butane feed (Adeeva *et al.* (48) and Tábora and Davis *et al.* (44) have independently reported a bimolecular mechanism for *n*-butane isomerization on SZ at 130 and 200°C, respectively) or depends on acid sites (not superacidic) alone to protonate *n*-butane (only active at high reaction temperatures).

Physical mixtures of different metal sources and zirconia were also studied for *n*-butane isomerization (Table 4). However, none of these show any activity above sulfated zirconia. These findings suggest that an intimate contact or close proximity between the metal site and the acid site is required for reactivity. From the proposed bifunctional

TABLE 4

Physical Mixtures of Various Solids Used for Catalytic Screening Experiments

Sulfated Fe_2O_3 + SZ	Fe_2O_3 + SZ
Sulfated MnO + SZ	MnO + SZ
Sulfated Fe_2O_3 + sulfated MnO + SZ	Fe_2O_3 + MnO + SZ
FZ (tetragonal)[a] + SZ	FeO(OH) + SZ
FZ (monoclinic)[a] + SZ	$Fe_2(SO_4)_3$ + SZ

[a] FZ, iron impregnated onto zirconia.

mechanism, it is noticeable that the butene generated from an oxidative dehydrogenation of *n*-butane must be protonated and react with another butene. This spillover mechanism could help reduce polymerization and the subsequent coking deactivation. Also the mechanism suggests that only a very small amount of butene is necessary. Formation of water from the oxidative dehydrogenation of *n*-butane and carbonaceous surface species contribute to the subsequent deactivation. Upon deactivation, all Brønsted acid sites are depleted as shown in Fig. 4b.

The nature of the metal sites (both the oxy and the iron (III) species) remains unclear. It is not unreasonable to suggest the formation of iron (III) sites in close proximity to acid sites through initial calcinations to 600°C that can catalyze the *n*-butane isomerization at 100°C. Upon air calcination to above 450°C, an even more active iron site is generated, denoted here as an iron oxy species. Because of the high-temperature air calcination, this iron species is tentatively assigned as a tetrahedral iron (IV) species and is proposed to be necessary for *n*-butane isomerization at 30°C. The exact nature of this high-valent iron species and how it is stabilized by the zirconia structure remain unclear at this time. Other high-oxidation-state iron oxo-compounds have also been reported for the functionalization of hydrocarbons, e.g., iron (IV) and manganese (IV) and (V) oxo-porphyrin complexes hydroxylate alkanes and epoxidize olefins under mild conditions (49–62).

CONCLUSIONS

Results from catalytic studies on SFMZ at 30 and 100°C indicate the presence of redox-active metal sites used for *n*-butane isomerization activity. Under high-temperature air calcination to above 450°C, a labile but reactive metal oxy site is generated and shown to be necessary for activity at 30°C. Activation in helium generates an iron (III) site, which is also very active for *n*-butane isomerization but only at higher temperatures, e.g., 100°C. These metal sites are believed to be responsible for the oxidative dehydrogenation of *n*-butane to butene. These sites are in close proximity to acid sites and the combination of metal site and acid site contributes to the proposed ''bifunctional/spillover'' mechanism for *n*-butane isomerization by SFMZ at all temperatures. Results from the temperature-programmed desorption studies also suggest the presence of the above-mentioned metal sites and show that they are responsible for the oxidation of the probe molecule to CO_2. It is also concluded that the desorption channels for various probe molecules on SZ and SFMZ are very different and none of them selectively probe only the acid site. More importantly, data from both the catalytic and the TPD experiments clearly rule out the postulation that superacidity contributes to the near room-temperature *n*-butane isomerization activity of SFMZ.

ACKNOWLEDGMENTS

Support for this work was provided by Akzo. We thank Professor R. J. Davis for helpful discussion and a preprint.

REFERENCES

1. Pines, H., ''The Chemistry of Catalytic Hydrocarbons Conversion.'' Academic Press, New York, 1981.
2. Corma, A., and Martinez, A., *Catal. Rev. Sci. Eng.* **35,** 483 (1993).
3. Corma, A., Juan-Rajadell, M. I., Lopez-Nicto, J. M., and Martinez, A., *Appl. Catal. A* **111,** 175 (1994).
4. Tanabe, K., Misono, M., Yoshio, O., and Hattori, H., ''New Solid Acids and Bases.'' Kodansha, Tokyo, 1989.
5. Misono, M., and Okuhara, T., *Chemtech* **Nov.,** 23 (1993).
6. Yamaguchi, T., *Appl. Catal.* **61,** 1 (1990).
7. Bearez, C., Chevalier, F., and Guisnet, M., *React. Kinet. Catal. Lett.* **22,** 405 (1983).
8. Guisnet, M., Avendano, F., Bearez, C., and Chevalier, F., *J. Chem. Soc., Chem. Commun.,* 336 (1985).
9. Bearez, C., Avendano, F., Chevalier, F., and Guisnet, M., *Bull. Soc. Chim. Fr.,* 346 (1985).
10. Takahashi, O., and Harttori, H., *J. Catal.* **68,** 132 (1981).
11. Na, K., Okuhara, T., and Misono, M., *Chem. Lett.* **7,** 1141 (1993).
12. Na, K., Okuhara, T., and Misono, M., *J. Chem. Soc., Faraday Trans.* **91,** 367 (1995).
13. Yamaguchi, T., Nakano, Y., and Tanabe, K., *Bull. Chem. Soc. Jpn.,* 51 (1978).
14. Hino, M., and Arata, K., *Chem. Lett.,* 1259 (1979).
15. Tanabe, K., Kayo, A., and Yamaguchi, T., *J. Chem. Soc., Chem. Commun.,* 602 (1981).
16. Kayo, A., Yamaguchi, T., and Tanabe, K., *J. Catal.* **83,** 99 (1983).
17. Yamaguchi, T., Jin, T., Ishida, I., and Tanabe, K., *Mater. Chem. Phys.* **17,** 3 (1986).
18. Arata, K., and Hino, H., *Appl. Catal.* **59,** 197 (1990).
19. Hino, M., and Arata, K., *J. Chem. Soc., Chem. Commun.,* 1148 (1979).
20. Hino, M., Kobayashi, S., and Arata, K., *J. Am. Chem. Soc.* **101,** 6439 (1979).
21. Hino, M., and Arata, K., *J. Chem. Soc., Chem. Commun.,* 851 (1980).
22. Arata, K., *Adv. Catal.* **37,** 165 (1990).
23. Davis, B. H., Keogh, R. A., and Srinivasan, R., *Catal. Today* **20,** 219 (1994).
24. Hino, M., and Arata, K., *Catal. Lett.* **30,** 25 (1995).
25. Adeeva, V., de Haan, J. W., Jänchen, J., Lei, G. D., Schünemann, V., van de Ven, L. J. M., Sachtler, W. M. H., and van Santen, R. A., *J. Catal.* **151,** 364 (1995).
26. Cheung, T. K., d'Itri, J. L., Lange, F. C., and Gates, B. C., *Catal. Lett.* **31,** 153 (1995).

27. Cheung, T. K., d'Itri, J. L., and Gates, B. C., *J. Catal.* **153,** 344 (1995).
28. Tábora, J. E., and Davis, R. J., *J. Chem. Soc., Faraday Trans.* **91,** 1825 (1995).
29. Yori, J. C., Luy, J. C., and Parera, J. M., *Catal. Today* **5,** 493 (1989).
30. Garin, F., Andriamasinoro, D., Abdulsamad, A., and Sommer, J., *J. Catal.* **131,** 199 (1991).
31. Hsu, C. Y., Heimbuch, C. R., Armes, C. T., and Gates, B. C., *J. Chem. Soc., Chem. Commun.,* 1645 (1992).
32. Jatia, A., Chang, C., MacLeod, J. D., Okubo, T., and Davis, M. E., *J. Catal.* **25,** 21 (1994).
33. Lin, C. H., and Hsu, C. Y., *J. Chem. Soc., Chem. Commun.,* 1479 (1992).
34. Parry, E. P., *J. Catal.* **2,** 371 (1963).
35. Morterra, C., Cerrato, G., Visca, M., and Lenti, D. M., *Chem. Mater.* **3,** 132 (1991).
36. Morterra, C., Cerrato, G., Emanuel, C., and Bolis, V., *J. Catal.* **142,** 349 (1993).
37. Nascimento, P., Akratopolpou, C., Oszagyan, M., Coudurier, G., Travers, C., Joly, J. F., and Vedrine, J. C., *in* "Proceedings, 10th International Congress on Catalysis, Budapest, 1992" (L. Guczi, F. Solymosi, and P. Tetenyi, Eds.), Vol. B, p. 1185. Elsevier, Amsterdam/New York, 1993.
38. Cheung, T. K., d'Itri, J. L., and Gates, B. C., *J. Catal.* **151,** 464 (1995).
39. Pinna, F., Signoretto, M., Strukul, G., Cerrato, G., and Morterra, C., *Catal. Lett.* **26,** 339 (1994).
40. Weisz, P. B., *Chemtech* **Aug.,** 498 (1973).
41. Pereira, C., and Gorte, R. J., *Appl. Catal. A: General* **90,** 145 (1992).
42. Tittensor, J. G., Gorte, R. J., and Chapman, D. M., *J. Catal.* **138,** 714 (1992).
43. Biaglow, A. I., Parrillo, D. J., and Gorte, R. J., *J. Catal.* **144,** 193 (1993).
44. Tábora, J. E., and Davis, R. J., manuscript in preparation.
45. Coelho, M. A., Resasco, D. E., Sikabwe, E. C., and White, R. L., *Catal. Lett.* **32,** 253 (1995).
46. Adeeva, V., Lei, G. D., and Sachtler, W. M. H., *Appl. Catal. A***118,** L11 (1994).
47. Zarkalis, A. S., Hsu, C. Y., and Gates, B. C., *Catal. Lett.* **29,** 235 (1994).
48. Adeeva, V., Lei, G. D., and Sachtler, W. M. H., *Catal. Lett.* **33,** 135 (1995).
49. Menage, S., Vincent, J. M., Lambeaux, C., Chottard, G., Grand, A., and Fontecave, M., *Inorg. Chem.* **32,** 4766 (1993).
50. Leising, R. A., Kim, J. H., Perez, M. A., and Que, L., *J. Am. Chem. Soc.* **115,** 9524 (1993).
51. Sorokin, A., Robert, A., and Meunier, B., *J. Am. Chem. Soc.* **115,** 7293 (1993).
52. Mansuy, D., *Coord. Chem. Rev.* **125,** 129 (1993).
53. Chin, D. H., Balch, A. L., and LaMar, G. N., *J. Am. Chem. Soc.* **102,** 1446 (1980).
54. Balch, A. L., Chan, Y. W., Cheng, R. J., LaMar, G. N., Latos-Grazynsky, L., and Renner, M. W., *J. Am. Chem. Soc.* **106,** 7779 (1984).
55. Balch, A. L., Latos-Grazynsky, L., and Renner, M. W., *J. Am. Chem. Soc.* **107,** 2983 (1985).
56. Groves, J. T., Haushalter, R. C., Nakamura, N., Nemo, T. E., and Evans, B. J., *J. Am. Chem. Soc.* **103,** 2884 (1981).
57. Groves, J. T., and Watanabe, Y., *J. Am. Chem. Soc.* **110,** 8443 (1988).
58. Groves, J. T., and Watanabe, Y., *J. Am. Chem. Soc.* **108,** 507 (1986).
59. Groves, J. T., and Viski, P., *J. Org. Chem.* **55,** 3628 (1990).
60. Groves, J. T., and Nemo, T. E., *J. Am. Chem. Soc.* **105,** 5786 (1983).
61. Barton, D. H. R., Beviere, S. D., Chavasiri, W., Csuhai, E., Doller, D., and Liu, W. G., *J. Am. Chem. Soc.* **114,** 2147 (1992).
62. Arasasingham, R. D., He, G. X., and Bruice, T. C., *J. Am. Chem. Soc.* **115,** 7985 (1993), and references therein.